LARGE EDDY SIMULATION OF THE TURBULENT FLOW PAST A BACKWARD FACING STEP

Isothermal flow and flows with heat transfer and property variations

RAVIKANTH AVANCHA AND RICHARD PLETCHER
Department of Mechanical Engineering
Iowa State University, Ames IA 50011

Abstract

The heat transfer and fluid mechanics of a turbulent separating and reattaching flow past a single-sided backward-facing step are studied using large eddy simulation. A fully coupled, low Mach number preconditioned, collocated-grid, central differenced, compressible, finite volume formulation was developed to conduct the simulations. A sixth-order compact filter was used to prevent pressure-velocity decoupling. A compressible version of the dynamic subgrid scale model was used to model the effects of the smaller eddies. Navier-Stokes characteristic boundary conditions designed by Poinsot and Lele were used to provide boundary conditions. The isothermal turbulent flow past the step, at a Reynolds number of 5,540 (based on the step height and upstream centerline velocity) and a Mach number of 0.006, was simulated to validate the formulation. Subsequently, the bottom wall downstream of the step was supplied with constant wall heat flux levels of 1.0, 2.0, and 3.0 kW/m^2. The viscous sub-layer played a critical role in controlling the heat transfer rate. Streamwise and wall-normal turbulent heat fluxes were of the same order of magnitude. The Reynolds analogy did not hold in the recirculation region. However, the Stanton number profiles showed a striking similarity with the fluctuating skin-friction profiles.

1. Introduction

Turbulent flows with separation and reattachment, in the presence of heat transfer, occur routinely in aircraft propulsion equipment, such as turbines and combustors, and cause large variations of local heat transfer coefficient as well as augmentation of overall heat transfer. The backward facing step geometry is well suited for investigation into the characteristics of flow separation, reattachment and recovery in the presence of an adverse pressure gradient. Most of the numerical calculations to date for this flow regime with

heat transfer have used two equation turbulence models like the $k-\epsilon$ and $k-\omega$ models with the Reynolds averaged Navier-Stokes (RANS) equations. Existing RANS approaches have not been successful in predicting all the flow features and heat transport mechanisms for this geometry. A summary of benchmark calculations [1] noted that only the results for streamwise velocity and dissipation agreed amongst all contributors, but substantial differences were noted for the wall-normal velocity, skin friction, Nusselt number, and wall temperatures. For the Nusselt number profiles, none of the methods produced a shape similar to the experimental results of [2]. There did not appear to be any consistency in the computed points of maximum Nusselt number and the reattachment point [1]. Many simulations in this study did not include the effects of property variations although large heat flux levels were used. Since RANS methods rely to a great extent on the modeling aspects, large variations in the quality of simulations are observed depending on the model assumptions. Little *ad-hoc* modeling is employed in large eddy simulation (LES), where the three-dimensional unsteady motion of the larger eddies is computed and subgrid-scale modeling is employed to account for the effects of the smaller eddies. Thus, the large eddy simulations presented in this work offer a way to better understand the effects of the heat transfer and property variations in separated flow regions at low speeds.

2. Governing Equations and Subgrid Scale Modeling

The Favre-filtered compressible Navier-Stokes (NS) equations, and the equation of state, in their non-dimensional form are given as:

$$\frac{\partial \overline{\rho}}{\partial t} + \frac{\partial \overline{\rho}\tilde{u}_j}{\partial x_j} = 0 \tag{1}$$

$$\frac{\partial \overline{\rho}\tilde{u}_i}{\partial t} + \frac{\partial \overline{\rho}\tilde{u}_i\tilde{u}_j}{\partial x_j} = -\frac{\partial \overline{p}}{\partial x_i} + \frac{\partial \overline{\sigma}_{ij}}{\partial x_j} - \frac{\partial \tau_{ij}}{\partial x_j} \tag{2}$$

$$\frac{\partial}{\partial t}(\overline{\rho}\tilde{T}) + \frac{\partial}{\partial x_j}(\overline{\rho}\tilde{u}_j\tilde{T}) = -\frac{\partial \overline{q}_j}{\partial x_j} - \frac{\partial Q_j}{\partial x_j} \tag{3}$$

$$\overline{p} = \overline{\rho}R\tilde{T} \tag{4}$$

where the viscous stress tensor and heat conduction vector are given as,

$$\overline{\sigma}_{ij} = \overline{\frac{\mu}{Re}\left(\frac{\partial u_i}{\partial x_j} + \frac{\partial u_j}{\partial x_i} - \frac{2}{3}\frac{\partial u_k}{\partial x_k}\delta_{ij}\right)} \quad ; \quad \overline{q}_j = -\overline{\frac{k}{Pr\,Re}\left(\frac{\partial T}{\partial x_j}\right)} \tag{5}$$

and the subgrid scale stress tensor and heat conduction vector are given as,

$$\tau_{ij} = \overline{\rho}(\widetilde{u_i u_j} - \tilde{u}_i\tilde{u}_j) \quad ; \quad Q_j = \overline{\rho}(\widetilde{u_j T} - \tilde{u}_j\tilde{T}) \tag{6}$$

The turbulent stress τ_{ij} and the turbulent heat flux Q_j have to be modeled in order to close the system of equations. The compressible extension [3] to the dynamic subgrid scale model [4] employing the Smagorinsky model as the base model has been used in this study. The compressible flow version of the Smagorinsky model is given as

$$\tau_{ij} = \frac{1}{3}\tau_{kk}\delta_{ij} - 2\mu_T(\tilde{S}_{ij} - \frac{1}{3}\tilde{S}_{kk}\delta_{ij}) \; ; \quad \left\{\tilde{S}_{ij} = \frac{1}{2}\left(\frac{\partial \tilde{u}_i}{\partial x_j} + \frac{\partial \tilde{u}_j}{\partial x_i}\right)\right\} \tag{7}$$

where μ_T is the eddy-viscosity, and $\tilde{S}_{ij}$ is the Favre-filtered strain rate tensor. $\tau_{kk} = 2C_I\bar{\rho}\Delta^2|\tilde{S}|^2$ is used to model the sub-grid scale turbulent kinetic energy, τ_{kk}, as proposed by [5]. For closure, μ_T is parameterized by equating the sub-grid scale energy production and dissipation, and the subgrid scale heat flux vector Q_j is modeled using a gradient-diffusion hypothesis, to obtain

$$\mu_T = C_s\bar{\rho}\Delta^2\sqrt{2\tilde{S}_{ij}\tilde{S}_{ij}} \quad ; \quad Q_j = -\frac{\bar{\rho}C_s\Delta^2|\tilde{S}|}{Pr_T}\frac{\partial \tilde{T}}{\partial x_j} \tag{8}$$

where C_s is a model parameter and Pr_T is the turbulent Prandtl number defined as the ratio of eddy-viscosity ν_T to eddy-diffusivity α_T. Both C_s and Pr_T are computed "dynamically". Δ is the filter width which is typically assumed to be a function of the grid resolution, and calculated as $\Delta_{av} = (\Delta x \Delta y \Delta z)^{1/3}$.

3. Numerical Procedure

A coupled finite volume procedure, in primitive variables $[p, u, v, w, T]$ was used to solve the filtered NS equations. The method was fully implicit, second order accurate in time, with advective terms disretized using second order central differences and viscous terms with fourth order central differences. Time derivative preconditioning [6] was incorporated to alleviate the stiffness and convergence problems associated with the computation of low Mach number flows using traditional compressible formulations. An all-speed strategy has thus evolved that enables the application of the same methodology to incompressible flows and compressible flows at low Mach numbers where effects of property variations need to be accounted for. Sixth order compact filtering [7] was used to eliminate the pressure-velocity decoupling peculiar to collocated-grid methods. The system of algebraic equations was solved using the strongly implicit procedure (SIP) [8, 9]. A code well optimized for performance on the CRAY T-90 was used to perform the large eddy simulations.

4. Simulation Details and Results

The computational domain for the large eddy simulations was designed to match the backward-facing step geometry from the particle tracking velocimetry (PTV) experiments [10] and is shown in Fig.1. The Reynolds number, based on the step height and upstream centerline velocity (which was also the reference velocity) was 5,540. Reference values of thermal conductivity, density and dynamic viscosity were obtained at the reference temperature, T_{ref}, of 293 K. The grid resolution used for the simulations was: (1) Upstream of step: $17 \times 31 \times 48$, (2) Downstream of step: $72 \times 46 \times 48$ in the streamwise, wall-normal and spanwise directions respectively. Non-uniform grids were employed in the wall-normal (y), and streamwise (x) directions as opposed to a uniform grid in the spanwise (z) direction. No-slip boundary conditions were enforced at the top and bottom solid walls. Periodicity of flow was assumed in the spanwise direction. The Navier-Stokes characteristic boundary condition strategy [11] was employed at the inflow and outflow boundaries. Turbulent inflow conditions for each time step of the simulation were provided by planes of data stored from an independent LES of a channel flow with the same Reynolds number and time step. For the simulations with heat transfer, the bottom wall downstream of the step was the only one supplied with a constant heat flux. The remaining walls were insulated (adiabatic conditions).

4.1. ISOTHERMAL FLOW CASE

The streamwise (Fig. 3), wall-normal (Fig. 4) and spanwise mean velocity distributions, and the respective root mean square fluctuations (Figs. 5, 6) from the simulation showed excellent agreement with experimental results. Third order moments also showed good qualitative agreement with the experiment. The mean reattachment length from the simulation was predicted to be 6.0 x/h, as compared with 6.51 x/h reported in the experiment. The simulations captured the presence of a smaller corner eddy in addition to the large recirculation bubble (Fig. 2). Details of the isothermal simulation and results have been presented in [12].

4.2. CONSTANT WALL HEAT FLUX CASES

Heat flux (q_w) levels of 1.0, 2.0, and 3.0 kW/m^2 corresponding to normalized heat flux, Q^+ ($= q_w/\rho_{ref}U_{ref}C_pT_{ref}$) levels of 0.0014, 0.0028, 0.0042 were supplied to the surface downstream of the step, yielding maximum T_{wall}/T_{bulk} ratios of about 1.7, 2.3, and 2.9, respectively. The bulk temperature profiles (Fig. 7) were in good agreement with analytical estimates based on an overall energy balance for the uniform heat flux condition. The

wall temperatures (Fig. 8) showed a dramatic increase downstream of the step, and reached their peak values in the neighborhood of the streamwise distance of $x/h \sim 2$. This increase in temperature is accompanied by a decrease in convective heat transfer (as evidenced by the Stanton number profiles in Fig. 9) and suggests that the air in this zone is almost in a "stagnant" state. The Stanton number, St $(= h/\rho_{ref} U_{ref} C_p)$ is a modified Nusselt number $(St = Nu/Re\,Pr)$, where $Nu = hL_y/k_b$, L_y is the step height, h is the convective heat transfer coefficient, and k_b is the bulk thermal conductivity. The Stanton number attains a maximum slightly upstream of reattachment, which is in agreement with [13], as opposed to results from several other studies that have indicated the location of the peak Stanton (or Nusselt number) to coincide with the mean reattachment point. In the region of reattachment, the impinging shear layer is responsible for the depression in the wall temperature around reattachment. Downstream of reattachment, linear increase of the wall temperature and the monotonic decrease in the mean Stanton number profiles is consistent with the growth of the thermal boundary layer following reattachment.

The Reynolds analogy does not hold in the mean sense, *i.e.*, the mean Stanton number profiles (Fig. 9) do not correlate with the mean skin friction profiles (Fig. 10). However, it is interesting to note that the mean Stanton number profiles show a more striking similarity with the fluctuating skin-friction profiles (Fig. 11) than they do with the profiles of the average absolute skin-friction (Fig. 12), or the mean skin friction. The high degree of correlation between the fluctuating skin-friction coefficient and Stanton number suggests that the correct velocity scale governing the strength of convective effects in the reattachment zone must be related to the velocity fluctuations rather than the mean velocity [13].

The bottom wall skin-friction coefficient (Fig. 10), in terms of normalized quantities can be written as $C_f = (2/Re)\,[(\mu/\rho)\,\partial u/\partial y]_w$. The influence of the wall temperatures for the three heat flux cases on the skin-friction coefficient is through the density and viscosity evaluated at the wall.

It is indicated in [13] that the streamwise turbulent heat flux is negligible as compared to the wall-normal turbulent heat flux. However, we show that the streamwise turbulent heat flux (Fig. 13), and the wall-normal turbulent heat flux (Fig. 14) are of the same order of magnitude. Probable reasons for their observation of negligible streamwise heat flux are that the heat flux levels in their work are an order of magnitude smaller and the Reynolds numbers are three to five times greater than the ones in this study.

Root mean square density fluctuations of up to 20 % were observed. At the peak wall temperatures for the three heat flux cases, the viscosity and thermal conductivity are roughly about 20%, 40% and 60% greater than

the values at the inlet, which are at the reference temperature of 293 K, thus demonstrating the need for property variations to be considered in calculations involving high heat fluxes.

5. Concluding Remarks

Large eddy simulations to study the heat transfer and fluid dynamics of the turbulent reattaching flow past a backward-facing step have been successfully conducted. The choice of the formulation enabled the inclusion of property variations, and facilitated the study at low Mach numbers. An increase in heat flux supplied to the bottom wall downstream of the step results in the heat transfer rate starting to be dominated by conduction as opposed to convection. Large variation in the wall temperature is observed, and the wall temperature attains a maximum close to the step face. The peak heat transfer rate occurs slightly upstream of reattachment. Streamwise and wall-normal turbulent heat fluxes are of the same order of magnitude. The Stanton number profiles correlate strongly with the fluctuating skin-friction profiles, and this observation underscores the importance of the near-wall region in determining the heat transfer rate.

6. Acknowledgments

The current research was partially supported by the Air Force Office of Scientific Research under Grant F49620-94-1-0168 and by the National Science Foundation under grants CTS-9414052 and CTS-9806989. The use of computer resources provided by the National Partnership for Advanced Computational Infrastructure at the San Diego Supercomputing Center is gratefully acknowledged.

References

1. Abrous, A., and Emery, A. F., 1996, Benchmark computational results for turbulent backward-facing step flow with heat transfer, HTD-Vol. 331, National Heat Transfer Conference, Vol. 9, ASME.
2. Mori, Y., Uchida, Y. and Sakai, K., 1986, A study of the time and spatial structure of heat transfer performances near the reattaching point of separated flows, *Procs. 8th Int. Heat Transfer Conference*, pp. 1083-1088.
3. Moin, P., Squires, K., Cabot, W., and Lee, S., 1991, A dynamic subgrid scale model for large eddy simulations of compressible turbulent flows, *Phys. Fluids A-Fluid*, Vol. 3, pp. 2746-2757.
4. Germano, M., Piomelli, U., Moin, P., and Cabot, W. H., 1991, A dynamic subgrid scale eddy viscosity model, *Phys. Fluids A-Fluid*, **3**, 1760-1765.
5. Yoshizawa, A., 1986, Statistical theory for compressible turbulent shear flows, with the application to subgrid modeling. *Phys. Fluids A-Fluid*, Vol. 5, pp. 3186-3196.
6. Pletcher, R. H. and Chen, K.-H., 1993, On solving the compressible Navier-Stokes equations for unsteady flows at very low Mach numbers, AIAA Paper 93-3368.

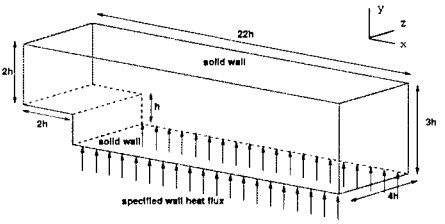

Figure 1. Backward-facing step geometry

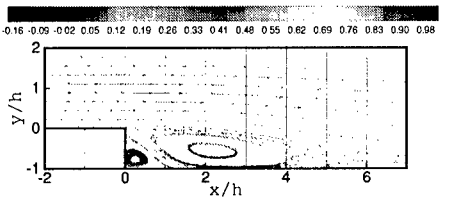

Figure 2. Mean streamlines

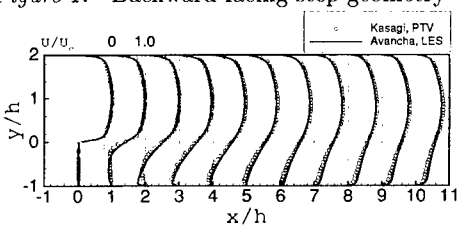

Figure 3. Mean streamwise velocity

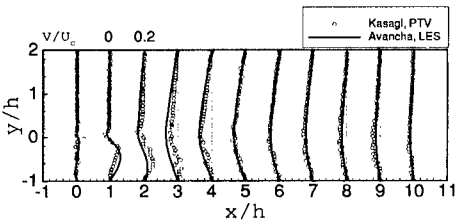

Figure 4. Mean wall-normal velocity

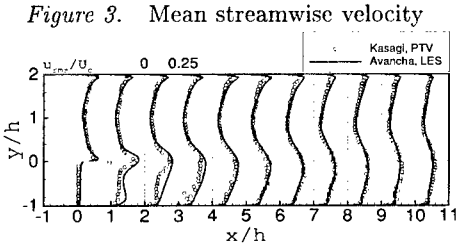

Figure 5. RMS streamwise velocity fluctuations

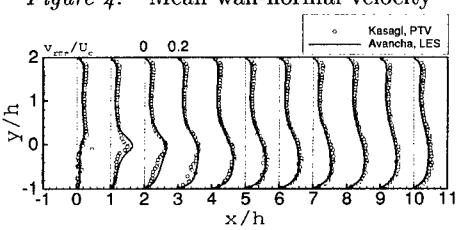

Figure 6. RMS wall-normal velocity fluctuations

7. Lele, S., 1992, Compact finite difference schemes with spectral-like resolution, *J. Comp. Phys.*, Vol. 103, pp. 16-42.
8. Stone, H. L., 1968, Iterative solution of implicit approximations of multidimensional partial differential equations. *SIAM J. Numer. Anal.*, Vol. 5, pp. 531-558.
9. Weinstein, H. G., Stone, H. L., and Kwan, T. V., 1969, Iterative procedure for solution of systems of parabolic and elliptic equations in three dimensions. *I & E C Fundamentals*, Vol. 8, pp. 281-287.
10. Kasagi, N., and Matsunaga, A., 1995, Three-dimensional particle-tracking velocimetry measurement of turbulence statistics and energy budget in a backward facing step flow, *Int. J. Heat and Fluid Fl.*, Vol. 16, pp. 477-485.
11. Poinsot, T. J., and Lele, S. K., 1992, Boundary conditions for direct simulations of compressible viscous flows, *J. Comp. Phys.*, Vol. 101, pp. 104-129.
12. Avancha, R., and Pletcher, R. H., 2000, Large eddy simulation of the turbulent flow past a backward facing step, AIAA 2000-0542, 38th Aerospace Sciences Meeting and Exhibit, 10-13 January 2000, Reno, NV.
13. Vogel, J. C., and Eaton, J. K., 1984, Heat transfer and fluid mechanics measurements in the turbulent reattaching flow behind a backward facing step, Report MD-44, Thermosciences Division, Department of Mechanical Engineering, Stanford University.

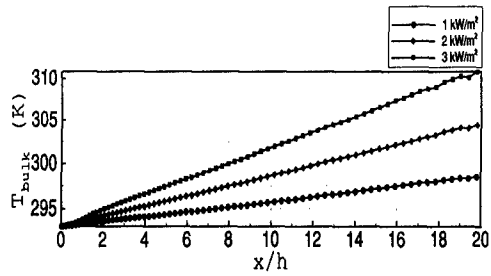

Figure 7. Bulk temperature

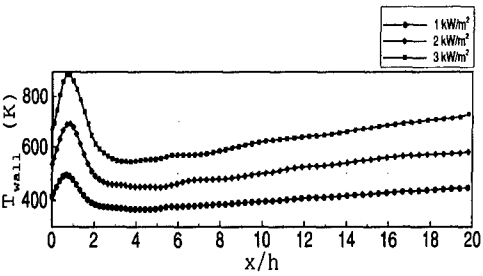

Figure 8. Wall temperature

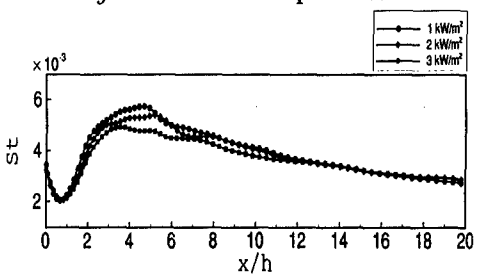

Figure 9. Stanton number

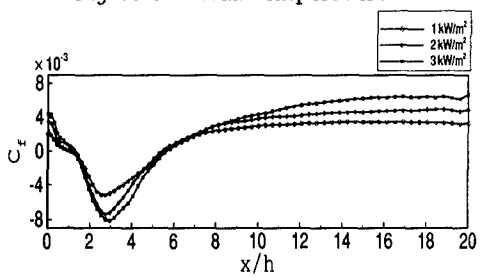

Figure 10. Skin-friction coefficient

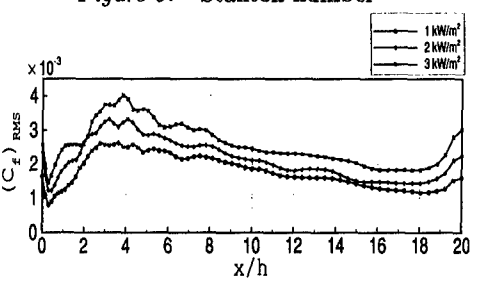

Figure 11. Fluctuating skin-friction

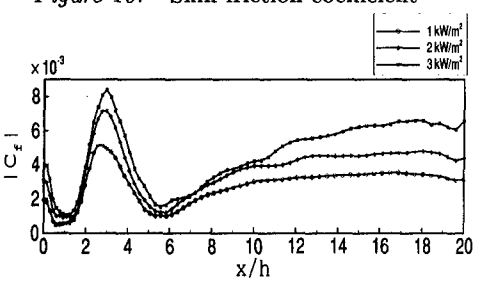

Figure 12. Average of absolute skin-friction

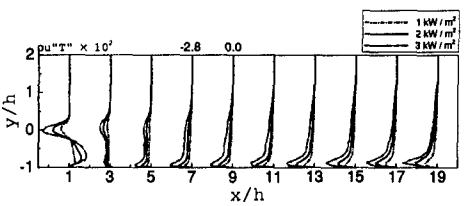

Figure 13. Streamwise turbulent heat flux

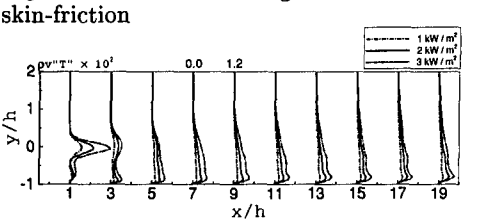

Figure 14. Vertical turbulent heat flux